Hydrogen Blending in Iberian Gas-Electricity Networks using Mixed Integer Linear Programming

Jorge Laguna Domínguez, Fco. Alberto Campos Fernández
Institute for Research in Technology (IIT)
ICAI School of Engineering, Comillas Pontifical University, Madrid, Spain
acampos@comillas.edu

Abstract—This paper develops an hourly optimization model coupling hydrogen (H_2) and natural-gas (NG) transport with electricity dispatch through combined-cycle gas turbines (CCGT). Mixed-gas nonlinearities are approximated using McCormick relaxations and a tangent-based pressure-flow approximation. An iterative concentration reconstruction and bound-refinement procedure reduces the mixing inconsistencies, while fixed flow directions and relaxed thermal commitments make the weekly solution tractable. A 2030 Iberian case study compares H2 mass-fraction limits from zero to 2.8% during a representative week. H2 utilization ranges from nearly 0% to 85.7%, showing that H2 injection potential strongly depends on project location, downstream gas demand, available NG dilution and network flow and pressure constraints. Increasing the maximum H_2 mass fraction from 0.7% to 2.8% raises avoided direct CO_2 emissions from 4.08 to 17.88 kt. Across the five cases, weekly Spanish CCGT energy rises from 589.4 to 646.9 GWh, a 9.8% increase between zero and 2.8% blending.

Keywords— H_2 blending, gas-electricity coupling, integer programming, McCormick relaxation, Iberian energy system.

I. INTRODUCTION

Combined-cycle gas turbines (CCGTs) link electricity dispatch to the operating limits of natural gas (NG) transmission networks. A generation schedule can be electrically admissible but unattainable when fuel delivery is constrained by pipeline capacities or nodal pressures [1]. Introducing hydrogen (H_2) in pipelines adds a second difficulty: the composition of the transported mixture is spatially heterogeneous and affects both pressure losses and the electricity produced from reconditioned CCGTs [2], [3]. The admissible H_2 blending limit, together with where, when, and how much H_2 can be injected, transported, and consumed while respecting the operational constraints of the coupled gas and electricity systems, must be carefully assessed. This paper addresses this issue for an aggregated representation of the Iberian energy system using a MILP model that jointly represents H_2–NG mixing and transport and CCGT electricity dispatch, with renewable H_2 availability treated exogenously.

A. Related work and contribution

Table I compares the main approaches presented in the related literature. For each reference, the table summarizes the gas mixture considered, the modelling objective, the mathematical formulation, the operating regime, the representation of the electricity grid, the solution method, the case study, and the main conclusions and contributions.

TABLE I. State of Art

Ref.	Gas / power coupling	Formulation and principal focus
[1]	NG / yes	MILP; security-constrained gas-electricity operation.
[4]	H2-NG / no	Nonlinear simulation; prescribed blend, steady and transient flow.
[2]	H2-NG / no	NLP; endogenous mixing and flow-direction consistency.
[3]	H2-NG / no	NLP; economic value and avoided carbon emissions.
[5]	H2-NG / no	NLP; compressor power and operating envelopes.
This work	H2-NG / yes	Hourly coupled optimization; MILP-based mixing refinement.

MILP: mixed-integer linear programming; NLP: nonlinear programming.

Overall, the reviewed literature can be grouped into three main categories. First, integrated gas–electricity models, such as [1], explicitly represent the operational coupling between both energy systems through gas-fired generation, but assume a homogeneous NG network and therefore do not address H_2 blending. Second, physically oriented H_2–NG network models, such as [2], represents H_2–NG mixtures and analyze the effect of H_2 on pressure and flow behavior, although without embedding these relationships into an optimization framework. Third, optimization-based H_2–NG blending models, represented by [3]–[5], endogenously determine H_2 transport and mixing while accounting for network constraints and, in some cases, economic, environmental, or compressor-related effects. However, these works mainly focus on the gas network itself and do not explicitly couple its operation with the electricity system. As can be seen in the table, the proposed model presented here lies at the intersection of these research streams, combining endogenous H_2–NG blending and gas-network hydraulics with electricity-system operation through CCGT dispatch. This combination constitutes the main modelling gap addressed in this work. Technically, the nonlinear gas-mixing and hydraulic relations are reformulated within a mixed-integer linear framework and solved through a practical iterative refinement procedure.

II. PROPOSED MODEL

This section first presents the assumptions adopted for the coupled gas-electricity model and then its mathematical formulation. Uppercase symbols represent inputs, whereas

lowercase variables or functions. All variables are positive except otherwise noticed.

A. Assumptions

Regarding the electricity system:

a) Each country is one electricity node.
b) Renewable H_2 availability is exogenous.

Regarding the gas logistics:

c) Gas-network operation is hourly and steady-state.
d) Pressure, mass flow and composition are constant within each hour.
e) Weymouth-type pressure losses are considered according to [6], while linepack, transients, elevation and minor losses are neglected.
f) Pipeline flow is isothermal, one-dimensional and horizontal.
g) Compressors are represented by an admissible pressure ratio, do not alter gas composition and have no explicit energy-consumption term.

Regarding the blending:

h) H_2 and NG mix homogeneously at nodes, move with the same bulk velocity and keep a uniform composition along each pipeline (arc).
i) The mixture is chemically inert.

B. Operating-cost objective

The total operating cost is minimized as:

$$\min c = c^E + \Delta T \cdot \sum_{i\in N, t\in T} (C_i^{NG} \cdot g_{it} + C_i^H \cdot h_{it}) + \Delta T \cdot C^{CO_2} \cdot E^{NG} \cdot \sum_{i\in W, t\in T} d_{it} \cdot (1 - x_{it}) \quad (1)$$

where c [€] is total operating cost and c^E [€] is the electricity-system cost excluding CCGT fuel. g_{it} and h_{it} [kg/s] are NG and H_2 injection flows, d_{it} [kg/s] is total gas withdrawal at CCGT nodes $W \subseteq N$, and x_{it} [-] is the nodal H_2 mass fraction. C_i^{NG} and C_i^H [€/kg] are NG and H_2 injection costs, C^{CO_2} [€/tCO₂] is the carbon price, E^{NG} [tCO₂/kgNG] is the direct NG emission factor, and ΔT [s] is the duration of each hourly period. The three terms in (1) represent electricity operation, gas supply and direct CO2 costs, respectively.

C. Electricity generation constraints

Demand-generation electricity balance, weekly hydropower, renewable production profiles and unit-commitment thermal constraints formulations are omitted in this paper, but can be drawn from [7].

D. Gas-network constraints

Let P and K be the pipeline and compressor sets. For node i, A_i^{in} and A_i^{out} denote arcs entering and leaving the node according to their reference orientation. The total-mixture flow f_{at} [kg/s] (free variable) satisfies:

$$\sum_{a\in A_i^{in}} f_{at} - \sum_{a\in A_i^{out}} f_{at} + g_{it} + h_{it} = d_{it} \quad (2)$$

H_2 is conserved independently. With z_{at} [-] denoting the H_2 mass fraction transported in arc a, the original constituent balance is:

$$\sum_{a\in A_i^{in}} z_{at} \cdot f_{at} - \sum_{a\in A_i^{out}} z_{at} \cdot f_{at} + h_{it} = x_{it} \cdot d_{it} \quad (3)$$

Equation (3) is nonlinear because it contains the products of concentration and flow on both transported and withdrawn gas.

For a pipeline $a = (i,j) \in P$, the transported composition must equal that of the actual upstream node taking into account the flow sign, i.e:

$$\begin{aligned} z_{at} &= x_{it} \text{ if } f_{at} \geq 0 \\ z_{at} &= x_{jt} \text{ if } f_{at} < 0 \end{aligned} \quad (4)$$

The conditional relation in (4) is reformulated with the binary direction variable $y_{at} \in \{0,1\}$ for $a = (i,j) \in P$ as follows:

$$\begin{aligned} -F_a^{\max} \cdot (1 - y_{at}) \leq f_{at} \leq F_a^{\max} \cdot y_{at} \\ -X^{\max} \cdot (1 - y_{at}) \leq z_{at} - x_{it} \leq X^{\max} \cdot (1 - y_{at}) \\ -X^{\max} \cdot y_{at} \leq z_{at} - x_{jt} \leq X^{\max} \cdot y_{at} \end{aligned} \quad (5)$$

Compressor arcs $a = (i,j) \in K$ are directed and preserve the inlet composition, i.e:

$$z_{at} = x_{it} \quad (6)$$

Pipeline $a = (i,j) \in P$ pressure losses follow the composition-dependent Weymouth relation [7]:

$$p_{it}^2 - p_{jt}^2 = W_a \cdot v(z_{at}) \cdot f_{at} \cdot |f_{at}| \quad (7)$$

where p_{it} [Pa] is nodal pressure, $v(z)$ [m²/s²] is the composition-dependent squared-speed-of-sound function and W_a [m⁻⁴] is the hydraulic coefficient. They are computed from the sound-speed inputs A^{NG} and A^H [m/s], the Darcy friction factor Λ_a [-], pipeline length L_a [m], diameter D_a [m] and cross-sectional area A_a [m²] of arc $a \in A$ as:

$$\begin{aligned} v(z) &= (A^{NG})^2 + [(A^H)^2 - (A^{NG})^2] \cdot z \\ W_a &= \frac{\Lambda_a \cdot L_a}{D_a \cdot A_a^2} \end{aligned} \quad (8)$$

Compressor arc $a = (i,j) \in K$ satisfies:

$$p_{it} \leq p_{jt} \leq R_a \cdot p_{it} \quad (9)$$

where R_a [-] is the maximum compressor pressure ratio. Equation (8) allows any pressure increase between zero and the installed compression capability.

The main operating limits are:

$$\begin{aligned} -F_a^{\max} \leq f_{at} \leq F_a^{\max},\ a \in P; \qquad 0 \leq f_{at} \leq F_a^{\max},\ a \in K \\ 0 \leq g_{it} \leq G_i^{\max}, 0 \leq h_{it} \leq H_i^{\max}, 0 \leq d_{it} \leq D_i^{\max} \\ P_i^{\min} \leq p_{it} \leq P_i^{\max}, 0 \leq x_{it} \leq X^{\max}, 0 \leq z_{at} \leq X^{\max} \end{aligned} \quad (10)$$

where $F_a^{\max}$ [kg/s] is the arc-flow limit; $G_i^{\max}$, $H_i^{\max}$ and $D_i^{\max}$ [kg/s] are the maximum NG injection, H2 injection and withdrawal at node i; $P_i^{\min}$ and $P_i^{\max}$ [Pa] are minimum and maximum bound of nodal pressure p_{it}; and $X^{\max}$ [-] is the maximum admissible H2 mass fraction.

E. Gas-electricity coupling

CCGT fuel conversion links gas withdrawals to electricity production:

$$q_{it} = E_i^{CC} \cdot [L^{NG} \cdot d_{it} + (L^H - L^{NG}) \cdot x_{it} \cdot d_{it}] \quad (11)$$

where q_{it} [MW] is CCGT electricity generation, E_i^{CC} [-] is conversion efficiency, and L^{NG} and L^H [MJ/kg] are the NG and H2 heating values. Because 1 MJ/s equals 1 MW, the gas-flow units in (11) directly yield electrical power. The product x_{it} times d_{it} is nonlinear and is treated in next section.

III. SOLUTION METHOD

Next subsections describe a linear approximation of the nonlinear constraints presented in previous section based on iterative McCormick relaxations [8].

A. Linear approximation of the proposed model

1) Linear approximation of the H2 mass balance

The two nonlinear products in (3) are isolated through the auxiliary decision variables u_{at} [kg/s], representing H_2 transported through arc a, and v_{it} [kg/s], representing H_2 withdrawn at node i:

$$u_{at} = z_{at} \cdot f_{at}, \qquad v_{it} = x_{it} \cdot d_{it} \tag{12}$$

Using these auxiliaries, (3) becomes the linear balance:

$$\sum_{a \in A_i^{in}} u_{at} - \sum_{a \in A_i^{out}} u_{at} + h_{it} = v_{it} \tag{13}$$

The equalities in (12) remain bilinear and are replaced by McCormick envelopes. For a generic product $w=x \cdot y$ with lower and upper bounds ($[X^L, X^U]$ for x and $[Y^L, Y^U]$ for y), the relaxation is:

$$\begin{aligned} w &\geq X^L \cdot y + Y^L \cdot x - X^L \cdot Y^L \\ w &\geq X^U \cdot y + Y^U \cdot x - X^U \cdot Y^U \\ w &\leq X^U \cdot y + Y^L \cdot x - X^U \cdot Y^L \\ w &\leq X^L \cdot y + Y^U \cdot x - X^L \cdot Y^U \end{aligned} \tag{14}$$

For the product in (12), the corresponding upper and lower bounds are those in (10). Note that the envelopes are convex relaxations, so the auxiliary variables need not equal the exact products inside these bounds.

2) Linear approximation of the CCGT thermal generation

According to (12), (11) is rewritten as:

$$q_{it} = E_i^{CC} \cdot [L^{NG} \cdot d_{it} + (L^H - L^{NG}) \cdot v_{it}] \tag{15}$$

4) Linear approximation of the Weymouth equation

The nonlinearities in (7) are treated sequentially. First, the auxiliary squared-pressure variable π_{it} [Pa²] replaces p_{it}^2:

$$\begin{aligned} &\pi_{it} = p_{it}^2, \qquad \left(P_i^{\min}\right)^2 \leq \pi_{it} \leq (P_i^{\max})^2 \\ &\pi_{it} \leq \pi_{jt} \leq R_a^2 \cdot \pi_{it}, \qquad a = (i,j) \in K \end{aligned} \tag{16}$$

This step is an exact variable reformulation and does not introduce any approximation.

Second, r_{at} [kg/s] represents $|f_{at}|$ in (7). Using the direction binary y_{at} from (5), its exact linear representation is:

$$\begin{aligned} f_{at} \leq r_{at} &\leq f_{at} + 2 \cdot F_a^{\max} \cdot (1 - y_{at}) \\ -f_{at} \leq r_{at} &\leq -f_{at} + 2 \cdot F_a^{\max} \cdot y_{at} \end{aligned} \tag{17}$$

Third, the auxiliary squared-flow variable s_{at} [(kg/s)²] approximates $sing(f_{at}) \cdot r_{at}^2$ by using a SOS2 interpolation, with λ_{akt} [-] as nonnegative interpolation weights:

$$\begin{aligned} &\sum_{k \in B} \lambda_{akt} = 1, \qquad \lambda_{akt} \geq 0 \text{ (SOS2)} \\ &r_{at} = \sum_{k \in B} R_{ak} \cdot \lambda_{akt}, \qquad s_{at} = \sum_{k \in B} S_{ak} \cdot \lambda_{akt} \end{aligned} \tag{18}$$

being B be the discretization points set, R_{ak} [kg/s] the input breakpoints of r_{at} and S_{ak} [(kg/s)²] define the corresponding square values.

Finally, b_{at} [(kg/s)²] is an auxiliary variable for the remaining product between composition and approximated squared flow (see equations (7) and (8)):

$$\begin{aligned} &b_{at} = z_{at} \cdot s_{at} \\ &0 \leq z_{at} \leq X^{\max}, \qquad 0 \leq s_{at} \leq (F_a^{\max})^2 \end{aligned} \tag{19}$$

The equality in (19) is relaxed with (14), using the concentration and squared-flow bounds.

For $a = (i,j) \in P$, the resulting Weymouth equation is therefore:

$$\pi_{it} - \pi_{jt} = W_a \cdot [(A^{NG})^2 \cdot s_{at} + ((A^H)^2 - (A^{NG})^2) \cdot b_{at}] \tag{20}$$

As can be seen, the final formulation is a MILP model.

B. Avoiding Exceeding Maximum Blending Admissible Limits

The first two McCormick relaxations in (12) might imply an H_2 share above the input X^{max} when concentration is reconstructed from flows f_{at}. To make the constraint independent of orientation, nonnegative positive- and reverse-direction components for f_{at} and u_{at} are introduced, together with the input $U_a^{max}=F_a^{max} \cdot X^{max}$ [kg/s]:

$$\begin{aligned} &f_{at} = f_{at}^p - f_{at}^n, \qquad u_{at} = u_{at}^p - u_{at}^n \\ &0 \leq f_{at}^p \leq F_a^{\max} \cdot y_{at}, \qquad 0 \leq f_{at}^n \leq F_a^{\max} \cdot (1 - y_{at}) \\ &0 \leq u_{at}^p \leq U_a^{\max} \cdot y_{at}, \qquad 0 \leq u_{at}^n \leq U_a^{\max} \cdot (1 - y_{at}) \\ &U_a^{\max} = F_a^{\max} \cdot X^{\max} \end{aligned} \tag{21}$$

Two auxiliary incoming-flow variables [kg/s] are defined in (22) for H2 and total-mixture flow; the nodal blending condition is:

$$\begin{aligned} u_{it}^{in} &= \sum_{a \in A_i^{in}} u_{at}^p + \sum_{a \in A_i^{out}} u_{at}^n + h_{it} \\ f_{it}^{in} &= \sum_{a \in A_i^{in}} f_{at}^p + \sum_{a \in A_i^{out}} f_{at}^n + g_{it} + h_{it} \end{aligned} \tag{22}$$

Then the next inequality avoids exceeding the maximum blending admissible limit when using the first two McCormick relaxations in (12):

$$u_{it}^{in} \leq X^{\max} \cdot f_{it}^{in} \tag{23}$$

Note that the hydraulic McCormick in (19) does not directly create an H2-limit exceedance, but its concentration interval is also tightened, as it will be seen in the next subsection.

B. A new Iterative Algorithm For H2-NG Blending Feasibility

Since the envelopes of the used McCormick relaxations do not impose the exact products, a feasible MILP may still be inconsistent with the physical H2 mixture. The following iterative procedure tightens the concentration domain while re-solving the complete coupled model.

Step 1: Initialization. Set iteration index k equal to 0, choose F^{min} [kg/s] and E^{tol} [-] as the flow and concentration tolerances, respectively.

Step 2: Solve the MILP subproblem. Consisting of (1) subject to the linear constraints in (2), (13), (5), (10), (15), (12), (19) (17)-(23) and the McCormick envelopes corresponding to the bilevel products in (12) and (19), and the electricity system constraints of [7].

Step 3: Computing and testing blending physical-consistency errors

After Step 2, incoming H_2 and total-mixture flows are reconstructed from the actual optimized concentration-flow products, not from relaxed u_{at} in (12). The reconstructed incoming-flow variables in (22) are computed at iteration k using the optimal solution obtained in previous step, as

follows: $\hat{h}$ and $\hat{f}$ [kg/s], concentration xphys [-] and consistency error e [-] are:

$$\hat{U}_{it} = \sum_{a \in A_i^{in}} z_{at} \cdot f_{at}^{p} + \sum_{a \in A_i^{out}} z_{at} \cdot f_{at}^{n} + h_{it}$$
$$\hat{F}_{it} = \sum_{a \in A_i^{in}} f_{at}^{p} + \sum_{a \in A_i^{out}} f_{at}^{n} + g_{it} + h_{it} \qquad (24)$$
$$X_{it}^{phys,k} = \frac{\hat{U}_{it}}{\hat{F}_{it}}, \qquad E_{it}^{k} = \left| x_{it} - X_{it}^{phys,k} \right|$$

A node-hour satisfies the consistency test when $E_{it}^{k} \leq E^{tol}$. Note that the ratio $X_{it}^{phys,k}$ is evaluated only when $\hat{F}_{it}$ exceeds F^{min}. Node-hour combinations below F^{min} are excluded from the consistency test because the ratio is numerically ill-conditioned and physically insignificant.

Step 4: Updating McCormick relaxations

For each inconsistent node-hour, the local concentration bounds $X_{it}^{L,k+1}$ and $X_{it}^{L,k+1}$ [-] to be used in the four inequalities in (14) for the bilinear products in (12) and (19), are computed as follows:

$$X_{it}^{L,k+1} = \max\left(0, \min\left(X_{it}^{k}, X_{it}^{phys,k}\right)\right)$$
$$X_{it}^{U,k+1} = \min\left(X^{\max}, \max\left(X_{it}^{k}, X_{it}^{phys,k}\right)\right) \qquad (25)$$

Then go to step 2.

IV. CASE STUDY

This case study represents week 43 of a 2030 scenario to examine autumn renewable generation and gas-fired dispatch. Five blending cases are compared through electricity production, gas-network constraints, H2 uptake and avoided emissions, followed by computational results.

A. Input data and scenarios

The network comprises 102 nodes and 111 arcs, including 19 CCGT nodes, 11 NG entries and eight H2 hubs. The gas-network representation retains the main transmission corridors and strategic interconnection points; nearby CCGTs and injection facilities are grouped at common nodes, while short secondary spurs and some parallel routes are simplified or omitted (see [9] for more details). CCGT capacity is 24.56 GW in Spain and 3.87 GW in Portugal. Historical 2023 REE/REN profiles are rescaled to the scenario annual energy assumptions presented in [9] and [10]. CCGT locations use ESIOS [11]. Gas data come from Enagas and REN from [12], [13] and [14].

The eight H2 hubs in Table IV aggregate eleven prospective projects detailed in [9], [15] and [16]. NG costs is 0.40 €/kg, approximately 29 €/MWh, within the 2024 MIBGAS month-ahead range [17]. Carbon is valued at 64.74 €/tCO2 [18], with an NG emission factor of 2.44 kgCO2/kgNG.

The Spain-to-Portugal electricity limit is 3.68 GW. French electricity exchanges are external supply/demand outputs, with marginal import costs increasing from 40 to 80 €/MWh and marginal export value decreasing from 80 to 40 €/MWh.

A 2.8% mass maximum limit is assumed, which corresponds approximately to 20% by volume, in line with [19]. Four alternative limits are 0, 0.7, 1.4 and 2.1%. The 2.8% case is the base case, and the zero-blending case is the reference for emission reductions. Table III summarizes other main inputs. The remaining are documented in [9].

TABLE III. MAIN CASE-STUDY INPUTS AND THEIR BASIS

Input	Adopted value / assumption	Basis
Electricity demand	335 / 82 TWh per year (ES / PT)	[9], [10]
Thermal fleet	ES: 5.25 GW nuclear; 1.30 GW coal. PT: neither.	[9]
Hydro / pumping	ES: 32 / 13 TWh; PT: 13 / 3.2 TWh; 80% round-trip efficiency.	[9]
Pressures	40-80 bar[1]; NG slack pressure 80 bar.	[12], [13]
Pipe / compressor	Friction factor 0.01; velocity cap 15 m/s; nominal ratio 1.4.	[9], [14]
Fuel costs	NG: 0.40 €/kg; H2: zero (technical-uptake scenario).	[9]
Heating values	NG: 49.2 MJ/kg; H2/NG heating-value ratio: 2.44.	[9]
Blending cases	Maximum H2 mass fraction: 0, 0.7, 1.4, 2.1 and 2.8%.	[9]

B. Electricity dispatch

Figure 1(a) shows hourly Spanish demand, CCGT energy and wind-plus-solar generation (onshore/offshore wind, photovoltaic and solar thermal). Panel (b) compares the five CCGT profiles and their weekly energy totals.

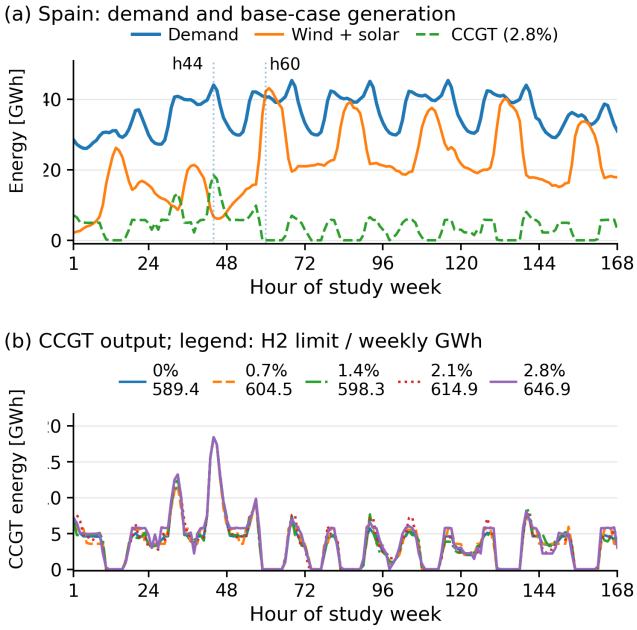


Fig. 1. Spanish hourly energy: (a) demand and selected technology generation; (b) CCGT sensitivity

At hour 60, wind-plus-solar reaches 42.33 GWh against 40.60 GWh of demand, with essentially zero CCGT output. At

[1] In the case studies, pressure inputs in bar are converted to pascals for the formulation in Section II; results are reported in bar for readability. The conversion is 1 bar = 10^5 Pa (and 1 bar^2 = 10^{10} Pa^2).

hour 44, demand is 44.09 GWh, wind-plus-solar is 6.62 GWh and CCGTs reach 18.43 GWh. CCGTs thus respond to residual requirements, alongside other generators, pumping and exchanges.

Despite similar peaks, weekly CCGT energy rises from 589.4 GWh without blending to 646.9 GWh at 2.8%, a 9.8% increase. Overlapping hourly curves therefore do not imply negligible energy changes.

C. Gas-network constraints

Figure 2 identifies constrained corridors, showing maximum weekly arc utilization and minimum nodal pressure. Solid and dashed arrows denote pipelines and compressor arcs, respectively.

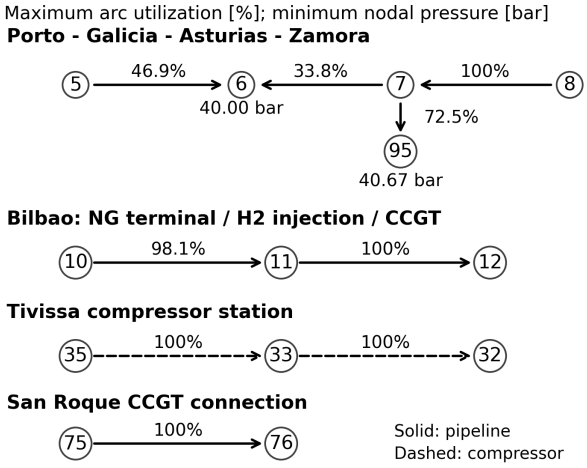


Fig. 2. Selected corridors in the 2.8% case

Five arcs reach 100% utilization and arc 10-11 reaches 98.1%. Node 6 reaches 40 bar while both supplying arcs remain below 50% utilization: pressure, rather than adjacent-arc capacity, binds. Node 95 retains only 0.67 bar of pressure margin.

Figure 3 pairs maximum weekly flow and simultaneous downstream pressure in pipeline 7-95 (Asturias-Zamora). Labels identify cases; inlet pressure is 80 bar and local H2 is zero. The dashed line marks the 40-bar limit.

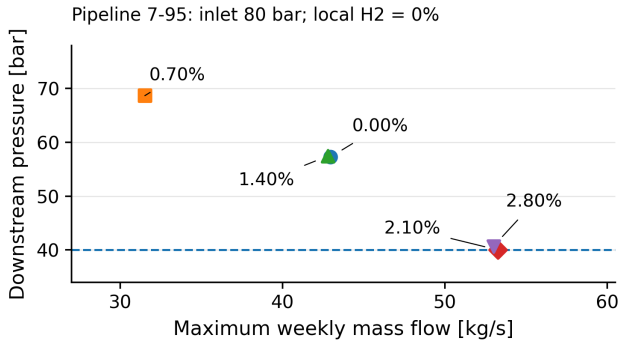


Fig. 3. Maximum flow and simultaneous downstream pressure in pipeline 7-95

Flow increases from 31.52 to about 53 kg/s as downstream pressure falls from 68.66 to approximately 40 bar. With no local H_2, this is consistent with non-local NG-flow redistribution, not a local composition effect.

D. Hydrogen uptake

Table IV reports injection caps and utilization (injected H2 divided by maximum 168-hour supply). Columns identify blending limits.

TABLE IV. H_2 INJECTION CAPACITY AND WEEKLY UTILIZATION

Location	Cap. kg/s	0.7%	1.4%	2.1%	2.8%
Sines	0.84	23.74	76.14	85.44	85.71
Bilbao	0.50	12.20	31.28	34.80	35.76
Aragon	3.61	4.07	3.88	9.22	34.32
Tarragona	0.75	0.03	1.12	3.57	5.75
Onda	0.61	0.04	0.00	0.01	0.00
Cartagena	0.50	35.22	49.18	50.04	11.88
Palos	1.43	18.55	38.38	58.29	71.01
Puertollano	1.74	0.70	4.02	20.75	29.90

At 2.8%, Sines and Palos reach 85.71% and 71.01% utilization, while Tarragona remains below 6% and Onda is unused. Sines has less injection capacity than Aragon but higher utilization. This supports location-dependent uptake, without isolating the individual network or dispatch constraints responsible.

Cartagena falls from 50.04% utilization at 2.1% blending to 11.88% at 2.8%, while Aragon rises from 9.22% to 34.32%. A higher ceiling therefore need not increase every project's utilization.

E. Avoided CO_2 emissions

Figure 4 plots weekly avoided direct CO_2 emissions against the blending limit, relative to the independently optimized zero-blend case. The left axis measures weekly avoided emissions in ktCO2, and the right axis gives their value in M€ at the adopted carbon price 64.74 €/tCO2.

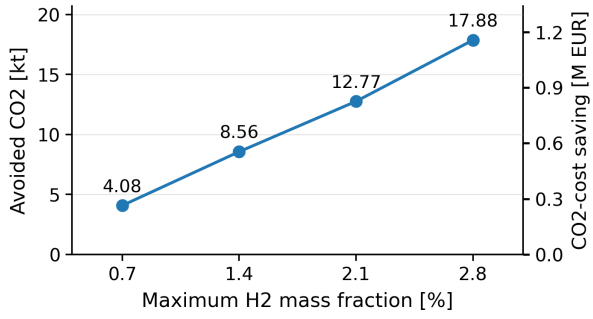


Fig. 4. Avoided direct CO_2 emissions and carbon-cost savings relative to zero blending

Avoided emissions rise from 4.077 to 17.876 ktCO2, worth 0.264 to 1.157 M€. This nearly proportional aggregate response coexists with non-monotonic project utilization (Table IV). These are direct-emission and carbon-cost differences, not life-cycle abatement or total system savings.

F. Computational results

GAMS 47.3.0 and IBM ILOG CPLEX 22.1.1.0 on Microsoft Windows 11, 64-bit, with Intel Core i7-9750H @ 2.60 GHz, 16 GB RAM and 12 threads have been used in this case estuy. The model has around 199,158 variables and 337,358 constraints before presolve. The algorithmic thresholds are F^{min}=0.001 kg/s and E^{tol}=0.005.

A single-hour test exceeded 24 h without reaching the 0.001 relative optimality gap. For this reason, a first run fixes f_{at} directions from an NG-only solve reaching 85% of CCGT capacity. This simplification also avoids SOS2 interpolation in (18) and instead uses tangent bounds of quadratic functions to model $sing(f_{at}) \cdot r_{at}^2$. In addition, thermal commitment is also relaxed. This reduces runtime by 87%, with objective and CCGT-energy changes below 0.1% and about 2%, respectively, respect to the integer model. With this simplification, each problem solved in step 2 of the algorithm is a LP. Table V gives wall-clock time and number of iterations for each scenario.

TABLE V. COMPUTATIONAL PERFORMANCE BY BLENDING CASE

Maximum H2 [%]	Total runtime [s]	Iterations
0	30	0
0.7	422	11
1.4	421	11
2.1	448	11
2.8	530	12

A dedicated convergence analysis is outside the scope of this paper. The numerical check concerns the mixing-consistency residual, not merely solver termination: linear constraints in each subproblem do not by themselves guarantee convergence of the outer concentration-update procedure.

V. CONCLUSIONS AND FUTURE WORK

This paper proposes a MLIP-based algorithm that jointly optimizes hourly electricity dispatch and steady-state H2-NG transport, linking both systems through CCGT fuel withdrawals and using McCormick relaxations with iterative concentration-bound refinement. In the Iberian case study, concentration limits, dilution, flow capacities and minimum pressures jointly determine H_2 uptake. A higher blending ceiling expands aggregate NG substitution, but does not increase every project's utilization. Hydraulic effects can also propagate to corridors with no local H_2 transport.

Fixed directions, tangent approximations and continuous commitment substantially reduce computational burden. Concentration reconstruction makes residual mixing inconsistencies visible and enables iterative improvement. Final physical-consistency certification depends on the maximum residual and convergence status. The reported 17.88 ktCO2 avoided at the highest blend is therefore a conditional screening result, not an investment or safety conclusion.

Future work should endogenize electrolyzer operation and H_2 storage, include compressor energy and performance, represent internal electricity transmission, and retain endogenous gas-flow directions using tighter formulations or decomposition. Pipeline-specific composition and pressure limits and more detailed topology would improve locational fidelity. Complete computational reporting and independent validation of mixing and hydraulic residuals are necessary before operational application.

REFERENCES

[1] C. M. Correa-Posada y P. Sánchez-Martın, «Security-Constrained Optimal Power and Natural-Gas Flow», *IEEE Trans. Power Syst.*, vol. 29, n.º 4, pp. 1780-1787, jul. 2014, doi: 10.1109/TPWRS.2014.2299714.

[2] S. R. Kazi, K. Sundar, S. Srinivasan, y A. Zlotnik, «Modeling and optimization of steady flow of natural gas and hydrogen mixtures in pipeline networks», *Int. J. Hydrog. Energy*, vol. 54, pp. 14-24, feb. 2024, doi: 10.1016/j.ijhydene.2023.12.054.

[3] M. Sodwatana, S. R. Kazi, K. Sundar, y A. Zlotnik, «Optimization of Hydrogen Blending in Natural Gas Networks for Carbon Emissions Reduction», en *2023 American Control Conference (ACC)*, may 2023, pp. 1229-1236. doi: 10.23919/ACC55779.2023.10156202.

[4] S. Elaoud, Z. Hafsi, y L. Hadj-Taieb, «Numerical modelling of hydrogen-natural gas mixtures flows in looped networks», *J. Pet. Sci. Eng.*, vol. 159, pp. 532-541, nov. 2017, doi: 10.1016/j.petrol.2017.09.063.

[5] B. Zhang *et al.*, «Influence of hydrogen blending on the operation of natural gas pipeline network considering the compressor power optimization», *Appl. Energy*, vol. 358, p. 122594, mar. 2024, doi: 10.1016/j.apenergy.2023.122594.

[6] R. Z. Ríos-Mercado y C. Borraz-Sánchez, «Optimization problems in natural gas transportation systems: A state-of-the-art review», *Appl. Energy*, vol. 147, pp. 536-555, jun. 2015, doi: 10.1016/j.apenergy.2015.03.017.

[7] P. González, J. Villar, C. Díaz, y Fco. A. Campos, «A conjectural supply function equilibrium in energy and reserve for a weekly horizon», en *2015 12th International Conference on the European Energy Market (EEM)*, may 2015, pp. 1-5. doi: 10.1109/EEM.2015.7216658.

[8] G. P. McCormick, «Computability of global solutions to factorable nonconvex programs: Part I — Convex underestimating problems», *Math. Program.*, vol. 10, n.º 1, pp. 147-175, dic. 1976, doi: 10.1007/BF01580665.

[9] J. Laguna Domínguez, «Modeling and Optimization of Hydrogen Transport in Reusable Gas Networks: Application to the Iberian Peninsula», B.Sc. thesis, Universidad Pontificia Comillas, Madrid, Spain, 2026.

[10] MITECO, «Plan Nacional Integrado de Energía y Clima (PNIEC 2023-2030)», *Ministerio para la Transición Ecológica y el Reto Demográfico*. 2024. Accedido: 18 de agosto de 2026. [En línea]. Disponible en: https://www.miteco.gob.es/es/energia/estrategia-normativa/pniec-23-30.html

[11] Red Eléctrica de España, «ESIOS: Maps of interest». Accedido: 11 de julio de 2026. [En línea]. Disponible en: https://www.esios.ree.es/es/mapas-de-interes

[12] Enagás, «Estaciones de compresión de gas». Accedido: 12 de julio de 2026. [En línea]. Disponible en: https://www.enagas.es/es/transicion-energetica/red-gasista/infraestructuras-gasistas/red-transporte/estaciones-compresion/

[13] REN Gasodutos, «PDIRG 2024-2033: Proposta». marzo de 2023. Accedido: 12 de julio de 2026. [En línea]. Disponible en: https://www.erse.pt/media/t0sfkmid/pdirg-2023.pdf

[14] Enagás, «Gasoductos: Infraestructuras gasistas». Accedido: 12 de julio de 2026. [En línea]. Disponible en: https://www.enagas.es/es/transicion-energetica/red-gasista/infraestructuras-gasistas/red-transporte/gasoductos/

[15] MITECO, «El MITECO adjudica 1.223 millones a siete proyectos de hidrógeno verde», *Ministerio para la Transición Ecológica y el Reto Demográfico*. junio de 2025. Accedido: 12 de julio de 2026. [En línea]. Disponible en: https://www.miteco.gob.es/es/prensa/ultimas-noticias/2025/junio/el-miteco-adjudica-1-223-millones-a-siete-proyectos-de-hidrogeno.html

[16] European Investment Bank, «Portugal: EIB finances Galp's Renewable Hydrogen and Biofuels projects in Sines with €430 million». 2025. Accedido: 12 de julio de 2026. [En línea]. Disponible en: https://www.eib.org/en/press/all/2025-107-eib-finances-galp-s-renewable-hydrogen-and-biofuels-projects-in-sines-with-eur430-million

[17] MIBGAS, «Informe anual del mercado organizado de gas 2024», 2025. Accedido: 24 de septiembre de 2026. [En línea]. Disponible en: https://www.mibgas.es/sites/default/files/mibgas-2024_informe_anual.pdf

[18] European Commission, «Report on the functioning of the European carbon market in 2024», COM(2025) 735 final, dic. 2025. Accedido: 16 de julio de 2026. [En línea]. Disponible en: https://climate.ec.europa.eu/document/download/ddc1b1de-652b-49ed-8f15-d9fa8badd39f_en?filename=com_2025_735_en.pdf

[19] J. Sánchez-Laínez *et al.*, «Enabling the injection of hydrogen in high-pressure gas grids: Investigation of the impact on materials and equipment», *Int. J. Hydrog. Energy*, vol. 52, pp. 1007-1018, ene. 2024, doi: 10.1016/j.ijhydene.2023.05.220.